

Optimization of Backscatter and Symmetry for Laser Fusion Experiments Using Multiple Tunable Wavelengths

J. E. Ralph¹, * P. Michel, B. J. MacGowan¹, D. J. Strozzi¹, N. B. Meezan, J.-M. Di Nicola, J. E. Heebner¹, V. J. Hernandez, L. Pelz, S. Yang, N. Lemos, L. Divol, A. Kemp, T. Chapman, S. F. Khan, O. L. Landen, J. D. Moody, R. P. J. Town, and M. J. Edwards
Lawrence Livermore National Laboratory, Livermore, California 94551, USA



(Received 31 May 2022; revised 9 August 2022; accepted 16 August 2022; published 17 October 2022)

A new additional wavelength-tuning capability has been implemented on the National Ignition Facility (NIF) laser allowing for unprecedented control of crossed-beam energy transfer (CBET) between all groups of beams for better performance of indirect-drive inertial confinement fusion (ICF) ignition experiments. In particular, this advance allows for negation and reversal of flow-induced CBET and the rebalancing of the intensity of different groups of beams within an indirect-drive (ICF) hohlraum. Experiments conducted at the NIF using a 1.1 MJ laser pulse with peak power of 390 TW demonstrate this high level of control through measurements of the precise changes to stimulated Brillouin scattering, typically driven by flow-induced CBET at the end of the pulse. Additionally, this new capability is shown to be able to predictably control gold-wall plasma expansion in the target driven by early-time flow-induced CBET. Estimates of early-time CBET from the wall expansion are shown to be consistent with simulation expectations. This new additional capability to control symmetry and backscatter expands the design space of current experiments and provides extra margin for increased laser energy in near-future experiments.

DOI: 10.1103/PhysRevApplied.18.044040

Inertial confinement fusion (ICF) consists of compressing and heating small targets containing mixtures of hydrogen isotopes [typically deuterium and tritium (DT)] in order to achieve thermonuclear fusion [1]. In the “indirect-drive” approach [2,3], a capsule containing the DT fuel is placed inside a “hohlraum,” a usually cylindrical cavity made of a high atomic number (Z) element (typically gold); a large number of laser beams enter through entrance holes at either end and deposit their energy in the gold wall, which then emits strong and uniform x-ray radiation that compresses the DT capsule. ICF experiments at the National Ignition Facility (NIF) [4] have recently achieved a “burning plasma” state, where the primary heating of the nuclear fuel is from the fusion reactions [5].

ICF experiments are often prone to laser-plasma instabilities (LPI), which can deteriorate the hohlraum performance by reducing the laser energy deposition (e.g., via backscatter instabilities) or degrading its symmetry. The hohlraum designs used over the last 5–10 years for experiments at the NIF use low hohlraum gas-fill densities ($\leq 0.6 \text{ mg cm}^{-3}$), which have been shown to largely eliminate backscatter from stimulated Raman scattering (SRS) that was present in the original designs at levels up to approximately 15%–20% of the total laser energy [6,7]. However, low gas-fill hohlraums tend to have a more prominent

wall plasma expansion inside the hohlraum, as shown in Fig. 1(a). These “gold bubbles,” driven by the “outer” beams propagating at 44.5° and 50° from the hohlraum axis, provide an environment prone to stimulated Brillouin scattering (SBS) for these outer beams. Indeed, the ion acoustic waves (IAWs) that are driven by SBS are very weakly damped in high- Z plasmas where the ion thermal velocity is much smaller than the acoustic velocity, making Landau damping of the waves ineffective [8]. In experiments at the NIF, SBS has tended to appear late in the pulse, when the gold bubble has fully developed, as shown in Fig. 1(b). While usually not as detrimental as SRS in terms of potential coupling loss (typically representing at most a couple of percent of the total laser energy), SBS poses a greater risk to the laser optics. Because its wavelength is approximately the same as that of the laser’s, it is more collimated than SRS, as its refraction through the plasma on the way back follows the refraction of the laser beams on their way in. Significant optics damage can occur even while the overall energy loss remains below 5% [9]. Because of the potential for optics damage and because it occurs near the end of the pulse, SBS is of particular concern for any potential scale-up of the current ICF experiments, at either the NIF (with higher laser energy) or any future facility.

On the other hand, crossed-beam energy transfer (CBET), which is also a LPI process, has been leveraged to help control the implosion symmetry of ICF

*ralph5@llnl.gov

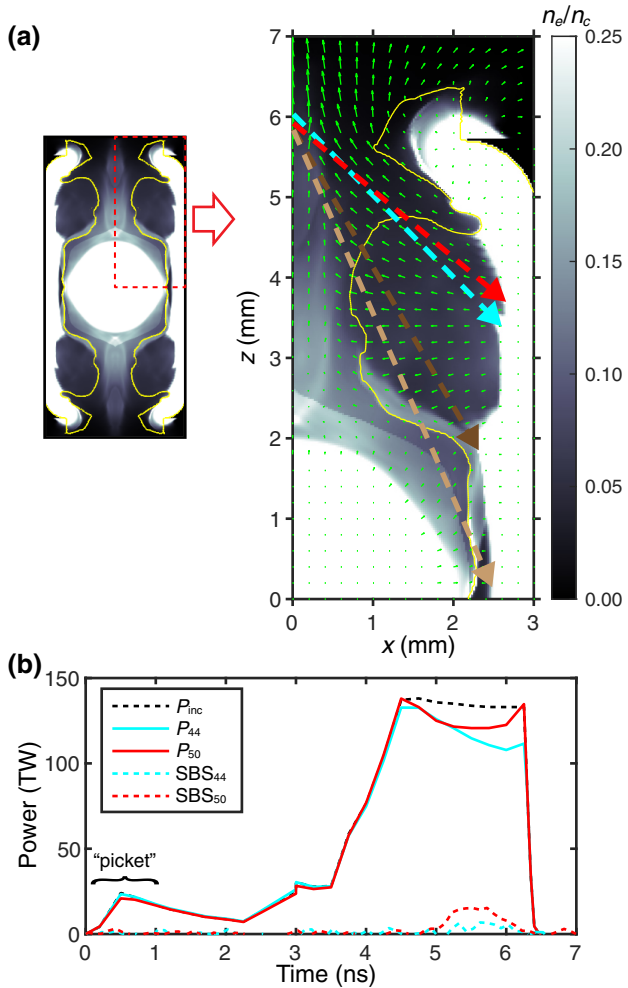


FIG. 1. (a) Hohlraum electron density n_e/n_c (grayscale) at $t = 6$ ns; the gold material contour is shown in yellow, and the four cones of NIF laser beams are represented by the dashed lines. The green arrows indicate the plasma flow direction and relative magnitude. (b) Incident laser power on the 44.5° and 50° cones (P_{inc}), power incident on the wall showing the flow-induced CBET ($\Delta\omega = 0$) from simulations on the 44.5° and 50° cones (P_{44} and P_{50}), and SBS measured on the two cones (SBS_{44} and SBS_{50}).

implosions. CBET, whereby laser beams overlapping in plasmas exchange energy with one another via scattering off IAWs [10–12], has been controlled and utilized at the NIF by independently adjusting the wavelengths of two [13–15] and then three [16,17] groups of laser beams.

In this article, we report on the implementation of a new (fourth) laser wavelength tuning capability at the NIF, providing an extra degree of freedom for the control of CBET in indirect-drive hohlraums. This new capability allows us to negate and reverse the CBET occurring near the hohlraum entrance holes due to plasma flow-induced Doppler shifts, and precisely adjust the energy balance between different groups of laser beams as they reach the

hohlraum wall. Precise tuning of wavelength differences between the 44.5° and 50° beams is shown to mitigate SBS and lead to a more uniform and azimuthally symmetric expansion of the gold bubble inside the hohlraum. Unlike previous SBS mitigation strategies such as the use of mixed ion species in the hohlraum wall to increase Landau damping of SBS-driven ion waves [18], SBS mitigation via CBET does not impact the hohlraum wall radiation spectrum and has, at most, a minor effect on the pole-waist drive symmetry. This new capability provides an additional margin to potentially increase the NIF laser energy and power to improve the performance and robustness of ICF implosions while keeping backscatter to acceptable levels.

The NIF's 192 laser beams are arranged in four cones at 23.5° , 30° , 44.5° , and 50° from the hohlraum axis. The beams in the inner cones (23.5° and 30°) hit the hohlraum wall near its waist and the outer cone (44.5° and 50°) beams hit closer to the equator, as shown in Fig. 1(a), where the brown dashed lines represent the 23.5° and 30° cones and the cyan and red dashed lines the 44.5° and 50° cones, respectively.

CBET occurs anywhere high-intensity laser beams overlap in a flowing plasma. Estimating the total amount of energy transfer at the NIF requires a detailed understanding of the plasma conditions and overlap geometry while accounting for all possible interactions between the 96 overlapping beams at each entrance hole [14,19]. However, valuable physical insight can be obtained by simply considering the CBET scaling laws between two beams. For a pair of beams with frequencies ω_0, ω_1 and wave vectors $\mathbf{k}_0, \mathbf{k}_1$, the spatial amplification rate Γ for beam 1 (in m^{-1} , such that the intensity I_1 satisfies $dI_1/dz = \Gamma I_1$ along the beam propagation axis z) due to beam 0 in the presence of a plasma flow \mathbf{V} can be expressed in the fluid limit as [8,11]

$$\Gamma = \Gamma_{\text{res}} \frac{v^2}{(\Delta\omega - \Delta\mathbf{k} \cdot \mathbf{V} - \Delta k c_s)^2 + v^2}, \quad (1)$$

where $\Gamma_{\text{res}} = a_0^2 \Delta k c_s / (8k_0 \lambda_{\text{De}}^2 v)$ is the peak amplification rate at resonance. Resonance is obtained when the beat wave between beams 0 and 1 resonantly drives an IAW, for $\Delta\omega = \Delta k c_s + \Delta\mathbf{k} \cdot \mathbf{V}$ with $\Delta\mathbf{k} \cdot \mathbf{V}$ the plasma flow-induced Doppler shift. Here $a_0 = v_{\text{osc}}/c$ is the electron quiver velocity in the laser electric field normalized to c , $\Delta\mathbf{k} = \mathbf{k}_0 - \mathbf{k}_1$, $\Delta\omega = \omega_0 - \omega_1$, c_s is the sound speed, v the IAW damping, and λ_{De} the Debye length.

The entrance holes, where all 96 NIF beams overlap, are the main locations where CBET occurs. Because the plasma flow in these regions is directed outward along the hohlraum axis, the Doppler shift (from the reference frame of the flowing plasma) tends to make all beams blue-shifted in the plasma frame following $\omega_{\text{plasma}} = \omega_{\text{lab}} - \mathbf{k} \cdot \mathbf{V}$ with $-\mathbf{k} \cdot \mathbf{V} = kV \cos(\theta) > 0$, where k is the laser wave

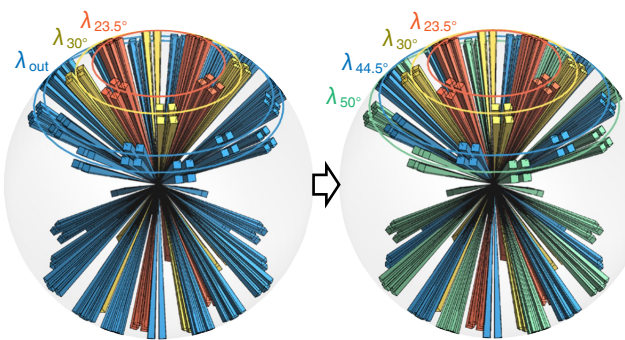


FIG. 2. Reconfiguration of the NIF laser front end to add a fourth tunable oscillator, leading to an independently tunable wavelength on each cone of beams.

number and θ the beam angle with respect to z . Beams at higher incidence angle are less blue-shifted than lower incidence angle beams in the plasma frame.

As a result, because of the outward flows at the entrance holes, CBET in the absence of laser-induced frequency shift tends to move energy out of the 44.5° beams and into the 50° beams. This has been robustly observed in simulations across almost all ICF designs, and (together with a 15% higher intensity on the 50° beams due to slightly smaller focal spots) is consistent with the systematic observation through almost all ICF experiments of a significantly larger SBS coming from the 50° beams than from the 44.5° beams. This is illustrated in Fig. 1(b), which shows the post-CBET power of the 44.5° and 50° cones calculated using the code Vampire [20] with plasma conditions provided by the radiative-hydrodynamics code Hydra [21] for the conditions of the experiments described below, with no frequency shifts imposed by the laser [i.e., $\Delta\omega = 0$ in Eq. (1): CBET and frequency shifts are merely due to flow-induced Doppler shifts in this case]. The measured SBS is also shown on the plot, with 50° SBS being approximately 3 times higher than the 44.5° SBS. The radial flow component from the gold bubble also leads to a net energy transfer from the outer to the inner beams for $\Delta\omega = 0$ further inside the hohlraum [22], as the inner beams penetrate the gold bubble and partially overlap theouters; this explains why the post-CBET power on both outer cones is lower than the incident.

In order to negate the flow-induced frequency shift responsible for increasing the intensity difference between the 44.5° and 50° beams as they hit the gold bubble plasma, the NIF laser front end was rearranged to accommodate a fourth, tunable oscillator, allowing independent control of the wavelength on each of the four cones of beams (Fig. 2). This change required a redesign of the legacy NIF Master Oscillator Room [4] to take advantage of recent advances in currently available, higher-performance fiber-based technology (e.g., acousto-optic modulators and ytterbium-doped amplifiers) and offer more flexibility with

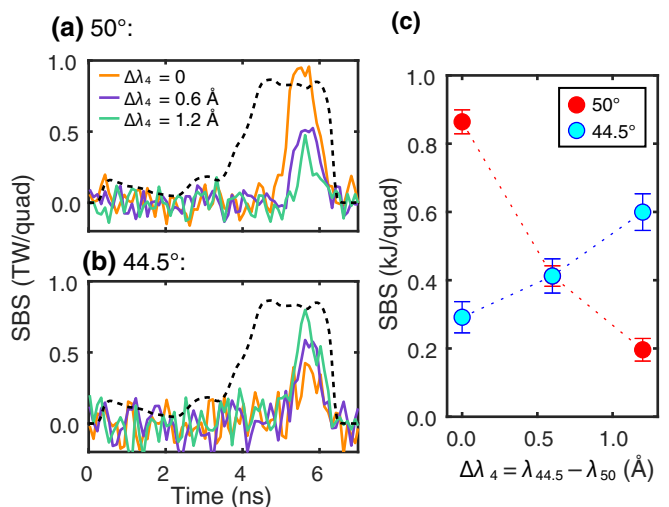


FIG. 3. Measured SBS on the 44.5° versus 50° beams for three different wavelength shifts $\Delta\lambda_4$ between the groups of beams: (a),(b) time-resolved measurements; (c) time-integrated measurements.

a tunable fourth oscillator [23], allowing independent control of the wavelength on each of the four cones of beams (Fig. 2).

To test this new capability, an experimental campaign is conducted using the same platform recently used for focused science campaigns at the NIF, such as hohlraum symmetry sensitivity studies or SBS mitigation using mixed ion species [18,24]; this platform has been shown to produce SBS levels that are high enough to be clearly measurable while remaining sufficiently far from the optics damage threshold. We use 5.75 mm diameter pure gold hohlraums filled with 0.3 mg/cm^3 and driven by a 1.1 MJ, 390 TW laser pulse [as shown in Fig. 1(b) for the outer cones of beams, peaking at 130 TW per cone]. A 0.91 mm outer-radius high-density carbon shell is used to assess symmetry.

Figure 3 shows the result of an experimental campaign at the NIF where a wavelength shift $\Delta\lambda_4 = \lambda_{44.5} - \lambda_{50}$ is introduced between the 44.5° and 50° beams [25]. SBS is measured using the NIF’s “drive diagnostics,” which collect the backscatter light through the lens on 58 of the 192 beams (with at least one measurement per quad), allowing averaging over azimuthal variations in the SBS signal [26]. The total SBS per quad is then extrapolated from these measurements in the lens based on near-backscatter imager measurements on one 50° quad [27].

The frequency shift between the 44.5° and 50° beams is done symmetrically with respect to the inner beam wavelength, i.e., $\lambda_{44} - \lambda_{\text{inn}} = \lambda_{\text{inn}} - \lambda_{50} = \Delta\lambda_4/2$, in order to prevent energy transfer between the inner and outer beams and keep the pole-waist symmetry constant. As $\Delta\lambda_4$ is increased, energy gets transferred from the 50° to the 44.5° beams, resulting in a clear decrease in 50° SBS

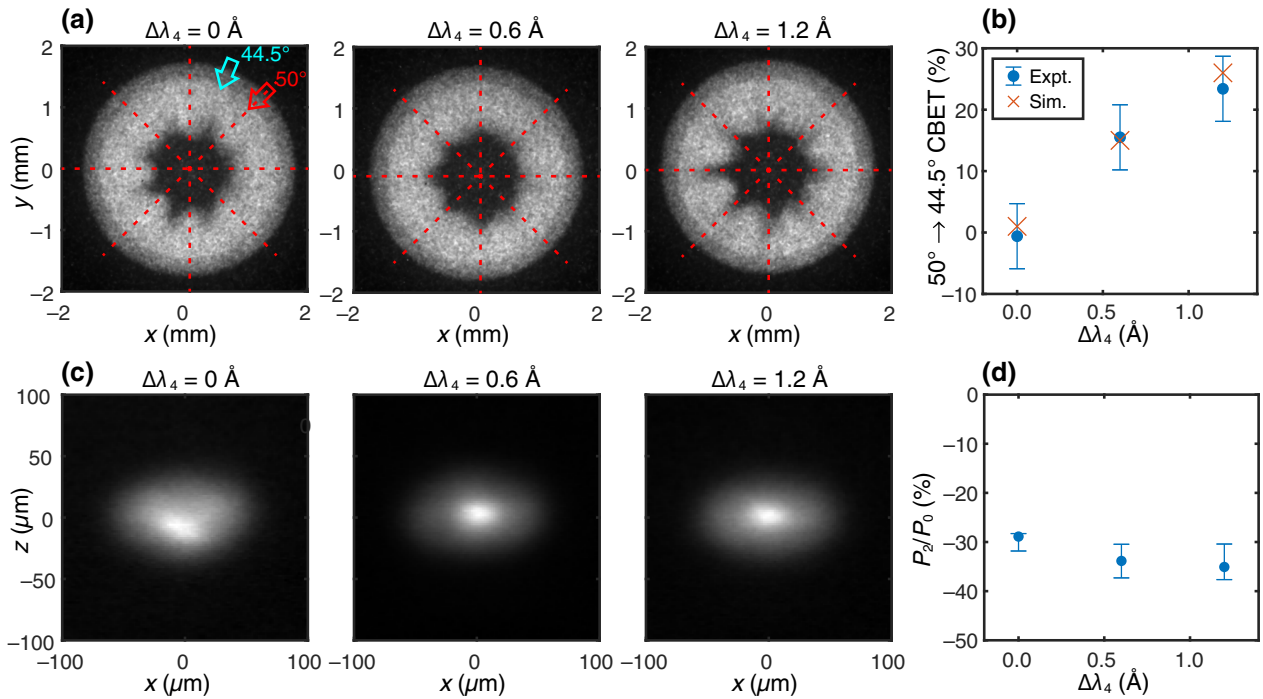


FIG. 4. (a) X-ray images of the gold bubble expansion viewed through the entrance hole, showing an eightfold pattern aligned with the 50° beams at $\Delta\lambda_4 = 0$, the 44.5° beams at $\Delta\lambda_4 = 1.2 \text{ \AA}$, and a smooth expansion at the intermediate 0.6 \AA . (b) CBET in the picket (relative energy transfer from the 44.5° to the 50° beams), inferred from the bubble expansion, and compared with simulations using Vampire. (c) Equatorial x-ray images of the imploded capsule self-emission at peak compression. (d) Pole-waist asymmetry (P_2/P_0) as a function of $\Delta\lambda_4$ [28].

and an increase in 44.5° SBS. An optimum is found near $\Delta\lambda_4 = 0.6 \text{ \AA}$. While the benefit in terms of laser coupling is marginal, re-equilibrating SBS between the 44.5° and 50° cones provides extra margin against potential optics damage on the 50° beam-lines at higher laser energies, which is the primary concern with outer-beam SBS at the NIF.

Energy transfer from the 50° to the 44.5° beams is also clearly visible on the gated x-ray radiographs shown in Fig. 4(a). These images show the emission from the gold bubbles driven by the 44.5° and 50° beams, which are also separated azimuthally. Figure 4(a) shows x-ray images looking straight down along the hohlraum axis through the upper laser entrance hole. Each pinhole image has a roughly 80-ps temporal resolution with peak spectral sensitivity around 10 keV (the Au L-band emission) using a $48 \mu\text{m}$ thick Ge filter. The entrance hole radius is initially 1.685 mm (compared to the hohlraum's 2.875 mm radius), which means that the near gold bubble needs to have expanded inwards by at least 1.19 mm before it becomes visible through the entrance hole. As indicated in the figure, the 16 quadruplets (quads) of 50° beams (8 quads from the upper hemisphere and 8 from the lower) hit the interior hohlraum wall near the laser entrance hole at azimuthal angles of $0 \pm n \times 45^\circ$ ($n \in \mathbb{N}$), whereas the 16 quads of 44.5° beams hit at $22.5^\circ \pm n \times 45^\circ$.

The gold bubble expansion velocity is largely dictated by the intensity in the “picket” of the laser pulse; here we define the picket as the first nanosecond of the laser pulse after turning on [Fig. 1(b)] [18,24,29,30]. For $\Delta\lambda_4 = 0$, and without flow-induced CBET in the picket, the 50° beams are 27% more intense than the 44.5° beams (at equal power) as they hit the wall, due to their 15% smaller area and smaller incidence angle. As a result, the gold bubble expansion is visibly more prominent at the azimuthal angles aligned with the 50° beams’ location (eightfold pattern) for $\Delta\lambda_4 = 0$. However, as $\Delta\lambda_4$ is increased, the wavelength-detuning-induced CBET [which is also effective in the picket, as the lower plasma temperature and higher density make up for the lower laser intensity; cf. Eq. (1) and Ref. [31]] reverses the trend: the eightfold pattern is aligned with the 44.5° beams at $\Delta\lambda_4 = 1.2 \text{ \AA}$, and the bubble is approximately smooth at 0.6 \AA , indicating an approximate balance between the two cones of beams.

Early-time CBET can be estimated using the established relationship between the velocity of the wall bubble and the picket fluence [30]. For a fixed hohlraum gas-fill pressure, we can relate the energy density deposited in the hohlraum wall by a laser beam, approximately E_p/A_w , where E_p is the beam’s energy in the picket (first 1 ns) pre-CBET and $A_w = A/\cos(\theta)$ its area on the wall (θ is the beam’s angle with respect to z and A ,

the cross-sectional area), to the expanding gold plasma kinetic energy, approximately V_b^2 , where V_b is the gold bubble expansion velocity. The expansion velocity is estimated by measuring the bubble radius using x-ray images like in Fig. 4(a) (taken at $t = 6.1$ ns), at times 4.6, 5.1, 5.6, and 6.1 ns. We assume the post-CBET picket energy for the 44.5° and 50° quads simply scales like $E_{p,44} + \Delta E(\Delta\lambda_4) = KA_{w,44}V_{44}^2$, $E_{p,50} - \Delta E(\Delta\lambda_4) = KA_{w,50}V_{50}^2$, with ΔE the wavelength-dependent energy transfer between the 44.5° and 50° beams and K a constant. Taking the ratio for equal *incident* picket energy between the 44.5° and 50° beams in the experiment ($E_{p,44} = E_{p,50} = E_p$) allows one to relate the relative CBET to the *measured* bubble velocities. Additionally, we assume the pre-CBET energy $E_p = (1/2)(KA_{w,44}V_{44}^2 + KA_{w,50}V_{50}^2)$ to get $\Delta E/E_p = [2A_{w,44}V_{44}^2/(A_{w,44}V_{44}^2 + A_{w,50}V_{50}^2)] - 1$. While simplistic, this estimate of picket CBET from the bubble expansion velocity is in good agreement with Vampire simulations, as shown in Fig. 4(b). In addition, we note that in this particular design, the same $\Delta\lambda_4$ shift that balances the SBS late in the peak of the pulse approximately equilibrates the gold bubble motion in the picket and smooths out the eightfold gold bubble azimuthal asymmetry. This is not always the case and depends on the details of the hohlraum design and laser pulse shape.

Finally, Figs. 4(c) and 4(d) show equatorial images of the imploded capsule x-ray self-emission at peak compression. This platform, which is typically used for dedicated science experiments and not for achieving high fusion yields [18,24], intrinsically comes with an oblate implosion (i.e., drive deficit from the hohlraum waist), which we do not aim to fix here. What the figure reveals is that tuning $\Delta\lambda_4$ does not have a significant effect on the pole-waist asymmetry P_2 . We quantify pole-waist asymmetry using the coefficient of the second Legendre polynomial P_2 , which is found by fitting the 17% contour of the x-ray images [32] shown in Fig. 4(c). This is in contrast to a previous SBS mitigation strategy where the gold wall was coated with a layer of Ta_2O_5 [18] in order to increase Landau damping of the SBS-driven IAWs, and which resulted in a significantly worse pole-waist asymmetry as well as a slight reduction in hohlraum drive due to the different radiation spectrum from Ta_2O_5 -coated versus uncoated gold.

In conclusion, we demonstrate that SBS in indirect-drive ICF experiments can be controlled through the implementation of a fourth independent and tunable oscillator, which brings a new degree of freedom for the control of CBET in experiments at the NIF. This new capability enables accurate control of the drive imbalance between the two cones of outer beams, and improves azimuthal symmetry of the gold bubble expansion inside the hohlraum. This provides additional leverage and margin to further optimize ICF hohlraums and safely push the NIF performance while keeping SBS under control.

ACKNOWLEDGMENTS

This work was performed under the auspices of the U.S. Department of Energy by Lawrence Livermore National Laboratory under Contract No. DE-AC52-07NA27344.

- [1] John Nuckolls, Lowell Wood, Albert Thiessen, and George Zimmerman, Laser compression of matter to super-high densities: Thermonuclear (ctr) applications, *Nature* **239**, 139 (1972).
- [2] John Lindl, Development of the indirect-drive approach to inertial confinement fusion and the target physics basis for ignition and gain, *Phys. Plasmas* **2**, 3933 (1995).
- [3] John D. Lindl, Peter Amendt, Richard L. Berger, S. Gail Glendinning, Siegfried H. Glenzer, Steven W. Haan, Robert L. Kauffman, Otto L. Landen, and Laurence J. Suter, The physics basis for ignition using indirect-drive targets on the National Ignition Facility, *Phys. Plasmas* **11**, 339 (2004).
- [4] M. L. Spaeth, *et al.*, Description of the NIF laser, *Fusion Sci. Technol.* **69**, 25 (2016).
- [5] A. B. Zylstra, *et al.*, Burning plasma achieved in inertial fusion, *Nature* **601**, 542 (2022).
- [6] N. B. Meezan, *et al.*, National ignition campaign hohlraum energetics, *Phys. Plasmas* (2010).
- [7] John Lindl, Otto Landen, John Edwards, and Ed Moses, Review of the national ignition campaign 2009-2012, *Phys. Plasmas* **21**, 020501 (2014).
- [8] Pierre Michel, Introduction to laser plasma interactions (Springer, 2022, in preparation).
- [9] T. Chapman, P. Michel, J.-M. G. Di Nicola, R. L. Berger, P. K. Whitman, J. D. Moody, K. R. Manes, M. L. Spaeth, M. A. Belyaev, C. A. Thomas, and B. J. MacGowan, Investigation and modeling of optics damage in high-power laser systems caused by light backscattered in plasma at the target, *J. Appl. Phys.* **125**, 033101 (2019).
- [10] William L. Kruer, Scott C. Wilks, Bedros B. Afeyan, and Robert K. Kirkwood, Energy transfer between crossing laser beams, *Phys. Plasmas* **3**, 382 (1996).
- [11] C. J. McKinstry, J. S. Liu, R. E. Giaccone, and H. X. Vu, Three-dimensional analysis of the power transfer between crossed laser beams, *Phys. Plasmas* **7**, 3 (1996).
- [12] R. K. Kirkwood, B. B. Afeyan, W. L. Kruer, B. J. MacGowan, J. D. Moody, D. S. Montgomery, D. M. Pennington, T. L. Weiland, and S. C. Wilks, Observation of Energy Transfer between Frequency-Mismatched Laser Beams in a Large-Scale Plasma, *Phys. Rev. Lett.* **76**, 2065 (1996).
- [13] P. Michel, L. Divol, E. A. Williams, S. Weber, C. A. Thomas, D. A. Callahan, S. W. Haan, J. D. Salmonson, S. Dixit, D. E. Hinkel, M. J. Edwards, B. J. MacGowan, J. D. Lindl, S. H. Glenzer, and L. J. Suter, Tuning the Implosion Symmetry of ICF Targets via Controlled Crossed-Beam Energy Transfer, *Phys. Rev. Lett.* **102**, 025004 (2009).
- [14] P. Michel, S. H. Glenzer, L. Divol, D. K. Bradley, D. Callahan, S. Dixit, S. Glenn, D. Hinkel, R. K. Kirkwood, J. L. Kline, W. L. Kruer, G. A. Kyrala, S. Le Pape, N. B. Meezan, R. Town, K. Widmann, E. A. Williams, B. J. MacGowan, J. Lindl, and L. J. Suter, Symmetry tuning via controlled crossed-beam energy transfer on the National Ignition Facility, *Phys. Plasmas* **17**, 056305 (2010).

- [15] S. H. Glenzer, *et al.*, Symmetric inertial confinement fusion implosions at ultra-high laser energies, *Science* **327**, 1228 (2010).
- [16] P. Michel, *et al.*, Three-wavelength scheme to optimize hohlraum coupling on the National Ignition Facility, *Phys. Rev. E* **83**, 046409 (2011).
- [17] J. D. Moody, *et al.*, Multistep redirection by cross-beam power transfer of ultrahigh-power lasers in a plasma, *Nat. Phys.* **8**, 344 (2012).
- [18] J. E. Ralph, A. Kemp, N. B. Meezan, R. L. Berger, D. Strozzi, B. J. MacGowan, O. Landen, N. Lemos, M. Belyaev, M. Biener, D. A. Callahan, T. Chapman, L. Divol, D. E. Hinkel, J. Moody, A. Nikroo, O. Jones, S. Schiaffino, M. Stadermann, and P. Michel, The effects of multispecies hohlraum walls on stimulated brillouin scattering, hohlraum dynamics, and beam propagation, *Phys. Plasmas* **28**, 072704 (2021).
- [19] P. Michel, L. Divol, E. A. Williams, C. A. Thomas, D. A. Callahan, S. Weber, S. W. Haan, J. D. Salmonson, N. B. Meezan, O. L. Landen, S. Dixit, D. E. Hinkel, M. J. Edwards, B. J. MacGowan, J. D. Lindl, S. H. Glenzer, and L. J. Suter, Energy transfer between laser beams crossing in ignition hohlraums, *Phys. Plasmas* **16**, 042702 (2009).
- [20] A. Colaïtis, T. Chapman, D. Strozzi, L. Divol, and P. Michel, A tesselation-based model for intensity estimation and laser plasma interactions calculations in three dimensions, *Phys. Plasmas* **25**, 033114 (2018).
- [21] M. M. Marinak, G. D. Kerbel, N. A. Gentile, O. Jones, D. Munro, S. Pollaine, T. R. Dittrich, and S. W. Haan, Three-dimensional Hydra simulations of National Ignition Facility targets, *Phys. Plasmas* **8**, 2275 (2001).
- [22] J. E. Ralph, *et al.*, Experimental room temperature hohlraum performance study on the National Ignition Facility, *Phys. Plasmas* **23**, 00 (2016).
- [23] Jean-Michel G. Di Nicola, *et al.*, in *High Power Lasers for Fusion Research VI*, Vol. 11666, edited by Abdul A. S. Awwal and Constantin L. Haefner, International Society for Optics and Photonics (SPIE, 2021).
- [24] N. Izumi, D. T. Woods, N. B. Meezan, J. D. Moody, O. L. Landen, L. Divol, Hui Chen, D. A. Callahan, M. Hohenberger, A. L. Kritcher, D. T. Casey, M. D. Rosen, J. S. Ross, M. B. Schneider, M. J. Edwards, and W. W. Hsing, Low mode implosion symmetry sensitivity in low gas-fill NIF cylindrical hohlraums, *Phys. Plasmas* **28**, 022706 (2021).
- [25] Wavelength shifts are quoted with respect to the “ 1ω ” fundamental laser wavelength of $1.054 \mu\text{m}$, since the wavelengths are adjusted in the fiber cavity section at 1ω . The shifts in the plasma, i.e., after frequency tripling, are a third of the ones quoted here. NIF shot numbers N200203-001-999, N200203-002-999, and N200213-002-999 correspond to $\Delta\lambda_4 = 0.0, 0.6$, and 1.0 \AA , respectively.
- [26] B. J. MacGowan, *et al.*, in *Anomalous Absorption Conference 2019, June 2019, Telluride, CO* (2019) <https://www.osti.gov/servlets/purl/1527292>.
- [27] J. D. Moody, *et al.*, Backscatter measurements for NIF ignition targets, *Rev. Sci. Instrum.* **81**, 10D921 (2010).
- [28] S. F. Khan, N. Izumi, S. Glenn, R. Tommasini, L. R. Benedetti, T. Ma, A. Pak, G. A. Kyrala, P. Springer, D. K. Bradley, and R. P. J. Town, Automated analysis of hot spot x-ray images at the National Ignition Facility, *Rev. Sci. Instrum.* **87**, 11E334 (2016).
- [29] J. E. Ralph, O. Landen, L. Divol, A. Pak, T. Ma, D. A. Callahan, A. L. Kritcher, T. Döppner, D. E. Hinkel, C. Jarrott, J. D. Moody, B. B. Pollock, O. Hurricane, and M. J. Edwards, The influence of hohlraum dynamics on implosion symmetry in indirect drive inertial confinement fusion experiments, *Phys. Plasmas* **25**, 082701 (2018).
- [30] D. A. Callahan, *et al.*, Exploring the limits of case-to-capsule ratio, pulse length, and picket energy for symmetric hohlraum drive on the National Ignition Facility laser, *Phys. Plasmas* **25**, 056305 (2018).
- [31] E. L. Dewald, *et al.*, Early-Time Symmetry Tuning in the Presence of Cross-Beam Energy Transfer in ICF Experiments on the National Ignition Facility, *Phys. Rev. Lett.* **111**, 235001 (2013).
- [32] G. A. Kyrala, S. Dixit, S. Glenzer, D. Kalantar, D. Bradley, N. Izumi, N. Meezan, O. L. Landen, D. Callahan, S. V. Weber, J. P. Holder, S. Glenn, M. J. Edwards, P. Bell, J. Kimbrough, J. Koch, R. Prasad, L. Suter, J. L. Kline, and J. Kilkenny, Measuring symmetry of implosions in cryogenic Hohlraums at the NIF using gated x-ray detectors (invited), *Review of Scientific Instruments* **81** (2010), 18th Topical Conference on High-Temperature Plasma Diagnostics, Wildwood, NJ, MAY 16-20, 2010.